EUROPEAN ORGANIZATION FOR NUCLEAR RESEARCH

CERN-EP/2003-068
October 24, 2003

Single- and Multi-Photon Events with Missing Energy in e^+e^- Collisions at LEP

The L3 Collaboration

Abstract

Single- and multi-photon events with missing energy are selected in 619 pb^{-1} of data collected by the L3 detector at LEP at centre-of-mass energies between 189 GeV and 209 GeV. The cross sections of the process $e^+e^- \rightarrow \nu\bar{\nu}\gamma(\gamma)$ are found to be in agreement with the Standard Model expectations, and the number of light neutrino species is determined, including lower energy data, to be $N_\nu = 2.98 \pm 0.05 \pm 0.04$. Selection results are given in the form of tables which can be used to test future models involving single- and multi-photon signatures at LEP. These final states are also predicted by models with large extra dimensions and by several supersymmetric models. No evidence for such models is found. Among others, lower limits between 1.5 TeV and 0.65 TeV are set, at 95% confidence level, on the new scale of gravity for the number of extra dimensions between 2 and 8.

Submitted to *Physics Letters B*

1 Introduction

In the Standard Model of the electroweak interactions [?] single- or multi-photon events with missing energy are produced via the reaction $e^+e^- \to \nu\bar{\nu}\gamma(\gamma)$ which proceeds through s-channel Z exchange and t-channel W exchange. The majority of such events are due to initial state radiation (ISR) from the incoming electrons and positrons[1]. The distribution of the recoil mass to the photon system, M_{rec}, is expected to peak around the Z mass in the s-channel, whereas ISR photons from the t-channel W exchange are expected to have a relatively flat energy distribution, peaked at low energies [?].

This Letter describes L3 results from the highest energy and luminosity LEP runs and improves upon and supersedes previous publications [?]. Other LEP experiments also reported similar studies [?]. The cross section measurement of the $e^+e^- \to \nu\bar{\nu}\gamma(\gamma)$ process is presented, as well as the direct measurement of the number of light neutrino species. Selection results are also given in the form of tables which can be used to test future models involving single- and multi-photon signatures at LEP.

The selected events are used to search for manifestations of Physics beyond the Standard Model, such as extra dimensions and Supersymmetry (SUSY). Models with large extra dimensions [?] predict a gravity scale, M_D, as low as the electroweak scale, naturally solving the hierarchy problem. Gravitons, G, are then produced in e^+e^- collisions through the process $e^+e^- \to \gamma G$, and escape detection, leading to a single-photon signature. Different mechanisms are suggested for symmetry breaking in SUSY models [?], which imply three different scenarios: "superlight", "light" and "heavy" gravitinos, $\tilde{G}$, with several single- or multi-photon and missing energy signatures. Results of generic searches for $e^+e^- \to XY \to YY\gamma$ and $e^+e^- \to XX \to YY\gamma\gamma$, where X and Y are new neutral invisible particles, are also discussed.

The main variables used in the selection of single- and multi-photon events are the photon energy, E_γ, polar angle, θ_γ, and transverse momentum, P_t^γ. Three event topologies are considered:

- High energy single-photon: a photon with $14^\circ < \theta_\gamma < 166^\circ$ and $P_t^\gamma > 0.02\sqrt{s}$. There should be no other photon with $E_\gamma > 1$ GeV.
- Multi-photon: at least two photons with $E_\gamma > 1$ GeV, with the most energetic in the region $14^\circ < \theta_\gamma < 166^\circ$ and the other in the region $11^\circ < \theta_\gamma < 169^\circ$. The transverse momentum of the multi-photon system should satisfy $P_t^{\gamma\gamma} > 0.02\sqrt{s}$.
- Low energy single-photon: a photon with $43^\circ < \theta_\gamma < 137^\circ$ and $0.008\sqrt{s} < P_t^\gamma < 0.02\sqrt{s}$. There should be no other photon with $E_\gamma > 1$ GeV.

The inclusion of the low energy single-photon sample significantly increases the sensitivity of the searches for extra dimensions and pair-produced gravitinos.

2 Data and Monte Carlo Samples

Data collected by the L3 detector [?] at LEP in the years from 1998 through 2000 are considered. They correspond to an integrated luminosity of 619 pb^{-1} at centre-of-mass energies $\sqrt{s} = 188.6 - 209.2$ GeV, as detailed in Table 1.

---

[1] A small fraction of photons originates from the t-channel W boson fusion in the $e^+e^- \to \nu_e\bar{\nu}_e\gamma(\gamma)$ process.

The following Monte Carlo generators are used to simulate Standard Model processes: `KKMC` [?] for $e^+e^- \rightarrow \nu\bar{\nu}\gamma(\gamma)$, `GGG` [?] for $e^+e^- \rightarrow \gamma\gamma(\gamma)$, `BHWIDE` [?] and `TEEGG` [?] for large and small angle Bhabha scattering, respectively, `DIAG36` [?] for $e^+e^- \rightarrow e^+e^-e^+e^-$ and `EXCALIBUR` [?] for $e^+e^- \rightarrow e^+e^-\nu\bar{\nu}$. The predictions of `KKMC` are checked with the `NUNUGPV` [?] generator. SUSY processes are simulated with the `SUSYGEN` [?] Monte Carlo program, for SUSY particles with masses up to the kinematic limit.

The L3 detector response is simulated using the `GEANT` program [?], which describes effects of energy loss, multiple scattering and showering in the detector. Time-dependent detector inefficiencies, as monitored during the data taking period, are included in the simulation.

3 Event Selection

Electrons and photons are reconstructed in the BGO crystal electromagnetic calorimeter (ECAL). It is accurately calibrated using an RFQ accelerator [?] and has an energy resolution $\sigma(E)/E = 0.035/\sqrt{E} \oplus 0.008$. Its barrel region subtends the polar angle range $43° < \theta < 137°$ while the endcap regions subtend the ranges $10° < \theta < 37°$ and $143° < \theta < 170°$. The region between the barrel and the endcaps is instrumented with a lead and scintillator fiber electromagnetic calorimeter (SPACAL), which is used as a veto counter to ensure the hermeticity of the detector. The fiducial volume of the tracking chamber (TEC), used to discriminate between photons and electrons, is $14° < \theta < 166°$.

Photon candidates are required to have an energy greater than 1 GeV and the shape of their energy deposition must be consistent with an electromagnetic shower. Bhabha and $e^+e^- \rightarrow \gamma\gamma(\gamma)$ events that are fully contained in the ECAL are used to check the particle identification efficiency and the energy resolution.

Single- and multi-photon events are accepted by calorimetric triggers monitored with a control sample of single-electron events. These are radiative Bhabha scattering events where one electron and a photon have a very low polar angle, and only a low energy electron is scattered at a large polar angle. They are accepted by a dedicated independent trigger requiring the coincidence of a charged track and a cluster in one of the luminosity monitors. Figure 1a shows the trigger efficiency as a function of the ECAL shower energy. In the barrel, it rises sharply at the energy threshold of a first trigger and reaches a plateau mainly determined by the presence of inactive channels [?]. With increasing energy additional triggers become active, resulting in a second threshold rise and a final plateau at efficiencies of $92.3 \pm 0.6\%$ in the barrel and $95.4 \pm 0.4\%$ in the endcaps. As the cross section of single-electron production decreases rapidly with the single-electron energy, the trigger performance study at high energies is complemented by studying Bhabha events selected using calibration data at the Z peak.

3.1 High Energy Single-Photon Selection

The selection of high energy single-photon events requires only one photon candidate in the barrel or endcaps with transverse momentum $P_t^\gamma > 0.02\sqrt{s}$. The energy not assigned to the identified photons must be less than 10 GeV and the energy measured in the SPACAL must be less than 7 GeV. There must be no tracks in the muon chambers and at most one ECAL cluster not identified as a photon is allowed in the event. Electron candidates are removed by requiring that no charged track reconstructed in the TEC matches the ECAL cluster.

The probability of photon conversion in the beam pipe and in the silicon microvertex detector is about 5% in the barrel region and increases rapidly at low polar angles, reaching about

20% at $\theta \approx 20^\circ$. To improve the selection efficiency in the presence of converted photons, the cut on the TEC tracks is released for events with $M_{rec} = 80 - 110$ GeV in the barrel and $M_{rec} = 80 - 140$ GeV in the endcaps. Photon candidates in the barrel region with M_{rec} outside this range are also accepted if they have two matching tracks with an azimuthal opening angle $\Delta\Phi_{tracks} < 15^\circ$. The distribution of $\Delta\Phi_{tracks}$ for photons accepted by this cut is presented in Figure 1b.

To reduce background from radiative Bhabha events at low polar angles and from the process $e^+e^- \rightarrow \gamma\gamma(\gamma)$, events with a transverse momentum less than 15 GeV are rejected if an energy cluster is observed in the forward calorimeters covering an angular range of $1.5^\circ - 10^\circ$, with an acoplanarity[2)] with the most energetic photon less than 30°. Furthermore, if a photon is detected with an acoplanarity less than 15° with a hadron calorimeter cluster, the energy of this cluster must be less than 3 GeV.

To reject cosmic ray background, no muon track segments are allowed in the event for photons with energy less than 40 GeV. If photons are more energetic, their ECAL showers leak into the time-of-flight system and its signals are required to be in time with the beam crossing within ±5 ns. Furthermore, an event is rejected if more than 20 hits are found in the central tracking chamber in a 1 cm road between any pair of energy depositions in the ECAL. The cosmic ray background in the event sample is estimated from studies of out-of-time events and amounts to 0.2%.

The noise in various subdetectors is studied using events randomly triggered at the beam crossing time. The resulting efficiency loss is 0.8%, and the Monte Carlo predictions are scaled accordingly.

In total, 1898 events are selected in data with 1905.1 expected from Monte Carlo. The purity of the selected $e^+e^- \rightarrow \nu\bar{\nu}\gamma(\gamma)$ sample is estimated to be 99.1%, with the main background coming from radiative Bhabha events and from the $e^+e^- \rightarrow \gamma\gamma(\gamma)$ process. Figures 2a and 2c show the distributions of M_{rec} and $|\cos\theta_\gamma|$. The numbers of events selected at different values of $\sqrt{s}$ are listed in Table 2, together with the Standard Model expectations. The efficiencies of the selection and the numbers of observed and expected events are given in Table 3 in bins of M_{rec} and $|\cos\theta_\gamma|$.

3.2 Multi-Photon Selection

Multi-photon candidates should have at least two photons with energy above 1 GeV and a global transverse momentum $P_t^{\gamma\gamma} > 0.02\sqrt{s}$. There should be no charged tracks matching any of the photon candidates.

The acoplanarity between the two most energetic photons is required to be greater than 2.5°. About 20% of the photon candidates are either near the calorimeter edges or have a dead channel in the 3×3 matrix around the crystal with the maximum energy deposition. For these events, the acoplanarity cut is relaxed to 10°. The distributions of the acoplanarity for events passing all other selection cuts are shown in Figures 1c and 1d.

In total, 101 multi-photon events are selected, with 114.8 expected from the Standard Model processes. The purity of the selected sample is 99.0%, with the main background coming from the $e^+e^- \rightarrow \gamma\gamma(\gamma)$ process. Figures 2b and 2d show the distributions of M_{rec} and of the energy of the second most energetic photon, E_{γ_2}. Table 2 gives the numbers of multi-photon events selected at different values of $\sqrt{s}$ together with the Standard Model expectations. The

---

[2)] Defined as the complement of the angle between the projections in the plane perpendicular to the beam axis.

efficiencies of the selection and the numbers of observed and expected events are given in Table 4 in bins of M_{rec} and E_{γ_2}, for the full sample and for the case in which both photons are in the barrel.

3.3 Low Energy Single-Photon Selection

This selection extends the P_t^γ range down to $0.008\sqrt{s}$. It covers only the barrel region where a single-photon trigger [?] is implemented with a threshold around 900 MeV, as shown in Figure 1a. In this region the background due to radiative Bhabha scattering increases, requiring additional cuts: no energy deposit is allowed in the forward calorimeters, there must be no other ECAL cluster with energy greater than 200 MeV, the energy in the hadron calorimeter must be less than 6 GeV and no tracks are allowed either in the TEC or in the muon chambers. To further reduce background from cosmic ray events not pointing to the interaction region, cuts on the transverse shape of the photon shower are also applied.

The numbers of selected and expected events are listed in Table 2. In total, 566 events are selected in data with an expectation of 577.8, where 124.2 events are expected from the $\mathrm{e^+e^-} \to \nu\bar{\nu}\gamma(\gamma)$ process and 447.2 from the $\mathrm{e^+e^-} \to \mathrm{e^+e^-}\gamma(\gamma)$ process. Figure 3a compares the photon energy spectrum with the Monte Carlo predictions. The normalisation of the $\mathrm{e^+e^-} \to \mathrm{e^+e^-}\gamma(\gamma)$ Monte Carlo is verified with a data sample selected with less stringent selection criteria.

Table 5 presents the numbers of observed and expected events, the efficiencies and the purities of the selected sample in bins of $|\cos\theta_\gamma|$ and $x_\gamma = E_\gamma/E_{beam}$, where E_{beam} is the beam energy. Single-photon events with $x_\gamma < 0.5$ from the combined high and low energy selections are listed, and the corresponding x_γ distribution is shown in Figure 3b.

4 Neutrino Production

The cross section of the process $\mathrm{e^+e^-} \to \nu\bar{\nu}\gamma(\gamma)$, where one or more photons are observed, is measured in the kinematic region $14° < \theta_\gamma < 166°$ and $P_t^\gamma > 0.02\sqrt{s}$ or $P_t^{\gamma\gamma} > 0.02\sqrt{s}$ using the high energy single-photon and the multi-photon samples. The average combined trigger and selection efficiency is estimated to be about 71% and is given in Table 6 as a function of $\sqrt{s}$ together with the results of the cross section measurement and the Standard Model expectations.

The systematic uncertainties on the cross section are listed in Table 7. The largest sources of systematics are the uncertainty on the determinations of the trigger efficiency and of the efficiency of the selection of converted photons, both due to the statistics of control data samples. Equally large is the uncertainty from Monte Carlo modelling, determined as the full difference between the efficiencies obtained using the `KKMC` and `NUNUGPV` Monte Carlo generators. Other uncertainties are due to the selection procedure, assigned by varying the selection criteria, the Monte Carlo statistics, the uncertainty on the measurement of the integrated luminosity, the level of background from Standard Model processes and cosmic rays and, finally, the accuracy of the ECAL calibration. All uncertainties, except that from Monte Carlo statistics, are fully correlated over different values of $\sqrt{s}$.

Figure 4 shows the measured $\mathrm{e^+e^-} \to \nu\bar{\nu}\gamma(\gamma)$ cross section as a function of $\sqrt{s}$, together with the Standard Model predictions and measurements at lower $\sqrt{s}$ [?]. The theoretical uncertainty on the predicted cross section is 1% [?]. The extrapolation to the total cross section of the $\mathrm{e^+e^-} \to \nu\bar{\nu}(\gamma)$ process, obtained using the `KKMC` program, is also shown in Figure 4.

To determine the number of light neutrino species, N_ν, a binned maximum likelihood fit is performed to the two dimensional distribution of M_{rec} *vs.* $|\cos\theta_\gamma|$ for events selected by the high energy single-photon and by the multi-photon selections. The expectations for different values of N_ν are obtained by a linear interpolation of the `KKMC` predictions for $N_\nu = 2, 3$ and 4. Due to the different contributions to the energy spectrum from the t-channel $\nu_e\bar{\nu}_e$ production and the s-channel $\nu\bar{\nu}$ production, this method is more powerful than using the total cross section measurement. Figure 5 shows the M_{rec} spectrum compared to the expectations for $N_\nu = 2, 3$ and 4. The result of the fit is:

$$N_\nu = 2.95 \pm 0.08(stat) \pm 0.03(syst) \pm 0.03(theory).$$

The systematic uncertainties are the same as for the cross section measurement. The last uncertainty includes the theoretical uncertainty on the expected cross section [?] as well as an additional uncertainty on the shape of the recoil mass spectrum, estimated by comparing `KKMC` with `NUNUGPV`. Combining this result with the L3 measurements at $\sqrt{s}$ around the Z resonance [?] and above [?], gives

$$N_\nu = 2.98 \pm 0.05(stat) \pm 0.04(syst).$$

This result is in agreement with the Z lineshape studies [?], while being sensitive to different systematic and theoretical uncertainties. It is more precise than the present world average of measurements relying on the single-photon method [?].

5 Searches for New Physics

5.1 Extra Dimensions

Gravitons expected in theories with n extra dimensions [?] are produced via the $e^+e^- \to \gamma G$ process and are undetected, giving rise to a single photon and missing energy signature. This reaction proceeds through s-channel photon exchange, t-channel electron exchange and four-particle contact interaction [?].

The efficiency for such a signal is derived in a x_γ *vs.* $|\cos\theta_\gamma|$ grid similar to that of Table 5 and, together with the analytical differential cross section [?], allows the calculation of the number of expected signal events as a function of $(1/M_D)^{n+2}$, to which the signal cross section is proportional. Effects of ISR are taken into account using the radiator function given in Reference ?. Since the photon energy spectrum from the $e^+e^- \to \gamma G$ reaction is expected to be soft, only single-photon events from the high and low energy samples with $x_\gamma < 0.5$ are considered. Effects of extra dimensions on the x_γ distribution are shown in Figure 3b. The two-dimensional distribution of x_γ *vs.* $|\cos\theta_\gamma|$ is fitted including a term proportional to $(1/M_D)^{n+2}$ with the results listed in Table 8. While similar searches were performed both at LEP [?, ?, ?] and the Tevatron [?], these results provide the most stringent limits for $n < 6$.

5.2 Model-Independent Searches

Single- and multi-photon events are used to investigate the $e^+e^- \to XY$ and $e^+e^- \to XX$ processes where X and Y are massive neutral undetectable particles and the $X \to Y\gamma$ decay occurs with a 100% branching ratio. Flat photon energy and polar angle distributions are assumed.

For the $\mathrm{e^+e^-} \rightarrow \mathrm{XY}$ search, a fit is performed to the M_{rec} distribution, whereas for the $\mathrm{e^+e^-} \rightarrow \mathrm{XX}$ channel, a discriminant variable is built [?] which includes M_{rec}, the energies of the two most energetic photons, their polar angles and the polar angle of the missing momentum vector. No deviation from the Standard Model expectations is observed and cross section limits are derived for all allowed values of the masses m_X and m_Y, in steps of 1 GeV. The observed and expected limits are shown in Figure 6 in the m_Y *vs.* m_X plane. The limits are obtained at $\sqrt{s} = 207$ GeV, data collected at lower $\sqrt{s}$ are included assuming the signal cross section to scale as β_0/s, where $\beta_0 = \sqrt{1 - 2(x_1 + x_2) + (x_1 - x_2)^2}$ with $x_1 = m_X^2/s$ and $x_2 = m_X^2/s$ or $x_2 = m_Y^2/s$ for the $\mathrm{e^+e^-} \rightarrow \mathrm{XX}$ and $\mathrm{e^+e^-} \rightarrow \mathrm{XY}$ searches, respectively$^{3)}$.

5.3 Neutralino Production in SUGRA Models

In gravity-mediated SUSY breaking models (SUGRA) the gravitino is heavy (100 GeV $\lesssim m_{\tilde{\mathrm{G}}} \lesssim$ 1 TeV) and does not play a role in the production and decay of SUSY particles. The lightest neutralino is the lightest supersymmetric particle (LSP), which is stable under the assumption of R-parity [?] conservation and escapes detection due to its weakly interacting nature. In this scenario, single- or multi-photon signatures arise from neutralino production through the processes $\mathrm{e^+e^-} \rightarrow \tilde{\chi}_1^0\tilde{\chi}_2^0$ and $\mathrm{e^+e^-} \rightarrow \tilde{\chi}_2^0\tilde{\chi}_2^0$ followed by the decay $\tilde{\chi}_2^0 \rightarrow \tilde{\chi}_1^0\gamma$ [?]. The signal topologies are similar to the ones assumed in the model-independent searches described above, and comparable cross section limits are derived.

The one-loop $\tilde{\chi}_2^0 \rightarrow \tilde{\chi}_1^0\gamma$ decay has a branching fraction close to 100% if one of the two neutralinos is pure photino and the other pure higgsino [?]. This scenario is suggested by an interpretation [?] of the rare $\mathrm{ee}\gamma\gamma$ event observed by CDF [?]. With this assumption, and using the results of the search for the $\mathrm{e^+e^-} \rightarrow \tilde{\chi}_2^0\tilde{\chi}_2^0$ process, a lower limit on the $\tilde{\chi}_2^0$ mass is calculated as a function of the right-handed scalar electron mass, $m_{\tilde{\mathrm{e}}_\mathrm{R}}$, using the most conservative cross section upper limit for any mass difference between $\tilde{\chi}_2^0$ and $\tilde{\chi}_1^0$ greater than 10 GeV. Two distinct scenarios are investigated: $m_{\tilde{\mathrm{e}}_\mathrm{L}} = m_{\tilde{\mathrm{e}}_\mathrm{R}}$ and $m_{\tilde{\mathrm{e}}_\mathrm{L}} \gg m_{\tilde{\mathrm{e}}_\mathrm{R}}$, where $m_{\tilde{\mathrm{e}}_\mathrm{L}}$ is the mass of the left-handed scalar electron. Figure 7 shows the excluded region in the $m_{\tilde{\chi}_2^0}$ *vs.* $m_{\tilde{\mathrm{e}}_\mathrm{R}}$ plane. The regions kinematically allowed from a study of the CDF event [?] are also indicated.

5.4 Superlight Gravitinos

When the scale of local supersymmetry breaking is decoupled from the breaking of global supersymmetry, as in no-scale supergravity models [?], the gravitino becomes "superlight" (10^{-6} eV $\lesssim m_{\tilde{\mathrm{G}}} \lesssim 10^{-4}$ eV) and is produced not only in SUSY particle decays but also directly, either in pairs [?] or associated with a neutralino [?]. Pair-production of gravitinos with ISR, $\mathrm{e^+e^-} \rightarrow \tilde{\mathrm{G}}\tilde{\mathrm{G}}\gamma$, leads to a single-photon signature which also arises from the $\mathrm{e^+e^-} \rightarrow \tilde{\mathrm{G}}\tilde{\chi}_1^0$ process with $\tilde{\chi}_1^0 \rightarrow \tilde{\mathrm{G}}\gamma$.

If the mass of the next-to-lightest supersymmetric particle (NLSP) is greater than $\sqrt{s}$, the process $\mathrm{e^+e^-} \rightarrow \tilde{\mathrm{G}}\tilde{\mathrm{G}}\gamma$ is the only reaction to produce SUSY particles. Its properties are similar to those of extra dimensions signals and its cross section is proportional to $1/m_{\tilde{\mathrm{G}}}^4$. A two-dimensional fit to the x_γ *vs.* $|\cos\theta_\gamma|$ distribution gives:

$$m_{\tilde{\mathrm{G}}} > 1.35 \times 10^{-5}\ \mathrm{eV},$$

at 95% confidence level, corresponding to a lower limit on the SUSY breaking scale $\sqrt{F} >$ 238 GeV. The expected lower limit on the gravitino mass is 1.32×10^{-5} eV.

[3)] We assume that the matrix elements of both processes do not depend on $\sqrt{s}$.

The reaction $e^+e^- \rightarrow \tilde{G}\tilde{\chi}^0_1$ proceeds through s-channel Z exchange and t-channel $\tilde{e}_{L,R}$ exchange. Efficiencies for this process range between 68% for $m_{\tilde{\chi}^0_1} = 0.5$ GeV and 75% at the kinematic limit. Cross section upper limits are derived at $\sqrt{s} = 207$ GeV from the photon energy spectrum and are shown in Figure 8a. Data collected at lower $\sqrt{s}$ are included assuming the signal cross section to scale as β^8 [?], where β is the neutralino relativistic velocity.

The no-scale SUGRA LNZ model [?] has only two free parameters, $m_{\tilde{G}}$ and $m_{\tilde{\chi}^0_1}$, and considers the neutralino to be almost pure bino and to be the NLSP. Its dominant decay channel is $\tilde{\chi}^0_1 \rightarrow \tilde{G}\gamma$, and a contribution from the decay into Z for $m_{\tilde{\chi}^0_1} \gtrsim 100$ GeV is taken into account. Figure 8c shows the excluded regions in the $m_{\tilde{G}}$ *vs.* $m_{\tilde{\chi}^0_1}$ plane. Gravitino masses below 10^{-5} eV are excluded for neutralino masses below 172 GeV.

5.5 The $e^+e^- \rightarrow \tilde{\chi}^0_1\tilde{\chi}^0_1 \rightarrow \tilde{G}\gamma\tilde{G}\gamma$ Process in GMSB Models

In models with gauge-mediated SUSY breaking (GMSB) [?], a light gravitino (10^{-2} eV $\lesssim m_{\tilde{G}} \lesssim 10^2$ eV) is the LSP. If the lightest neutralino is the NLSP, it decays predominantly through $\tilde{\chi}^0_1 \rightarrow \tilde{G}\gamma$, and pair-production of the lightest neutralino leads to a two-photon plus missing energy signature. The selection described in this Letter is devised for photons originating from the interaction point, and the following limits are derived under the assumption of a neutralino mean decay length shorter than 1 cm.

The same discriminant variable as in the $e^+e^- \rightarrow XX \rightarrow YY\gamma\gamma$ search is used and signal efficiencies are obtained which vary between 35% for $m_{\tilde{\chi}^0_1} = 0.5$ GeV and 70% for $m_{\tilde{\chi}^0_1} \gtrsim 100$ GeV. No deviations from the Standard Model are observed and upper limits on the cross section are derived as a function of $m_{\tilde{\chi}^0_1}$ at $\sqrt{s} = 207$ GeV, as displayed in Figure 8b. Data collected at lower $\sqrt{s}$ are included assuming the signal cross section to scale according to the MGM model [?]. The signal cross section predicted by the MGM model is also shown in Figure 8b. In this model, the neutralino is pure bino, and $m_{\tilde{e}_L} = 1.1 \times m_{\tilde{\chi}^0_1}$ and $m_{\tilde{e}_R} = 2.5 \times m_{\tilde{\chi}^0_1}$. A 95% confidence level limit on the neutralino mass is obtained as:

$$m_{\tilde{\chi}^0_1} > 99.5 \text{ GeV}.$$

Figure 8d shows the exclusion region in the $m_{\tilde{\chi}^0_1}$ *vs.* $m_{\tilde{e}_R}$ plane obtained after relaxing the mass relations of the MGM. The region suggested by an interpretation [?] of the $ee\gamma\gamma$ event observed by CDF is also shown. This interpretation is ruled out by this analysis.

6 Conclusions

The high performance BGO calorimeter and the dedicated triggers of the L3 detector are used to select events with one or more photons and missing energy in the high luminosity and centre-of-mass energy data sample collected at LEP. Single- and multi-photon events with transverse momentum as low as $0.008\sqrt{s}$ are considered. The numbers of selected events agree with the expectations from Standard Model processes and are given as a function of different phase space variables in the form of tables which can be used to test future models. The cross section for the process $e^+e^- \rightarrow \nu\bar{\nu}\gamma(\gamma)$ is measured with high precision as a function of $\sqrt{s}$, and is found to be in agreement with the Standard Model prediction. From these and lower energy data, the most precise direct determination of the number of light neutrino families is derived as:

$$N_\nu = 2.98 \pm 0.05(stat) \pm 0.04(syst).$$

Model independent searches for the production of new invisible massive particles in association with photons do not reveal any deviations from the Standard Model expectations and upper limits on the production cross sections are derived. Severe constraints are placed on models with large extra dimensions and several SUSY scenarios, excluding their manifestations at LEP.

The L3 Collaboration:

P.Achard,[20] O.Adriani,[17] M.Aguilar-Benitez,[24] J.Alcaraz,[24] G.Alemanni,[22] J.Allaby,[18] A.Aloisio,[28] M.G.Alviggi,[28] H.Anderhub,[46] V.P.Andreev,[6,33] F.Anselmo,[8] A.Arefiev,[27] T.Azemoon,[3] T.Aziz,[9] P.Bagnaia,[38] A.Bajo,[24] G.Baksay,[25] L.Baksay,[25] S.V.Baldew,[2] S.Banerjee,[9] Sw.Banerjee,[4] A.Barczyk,[46,44] R.Barillère,[18] P.Bartalini,[22] M.Basile,[8] N.Batalova,[43] R.Battiston,[32] A.Bay,[22] F.Becattini,[17] U.Becker,[13] F.Behner,[46] L.Bellucci,[17] R.Berbeco,[3] J.Berdugo,[24] P.Berges,[13] B.Bertucci,[32] B.L.Betev,[46] M.Biasini,[32] M.Biglietti,[28] A.Biland,[46] J.J.Blaising,[4] S.C.Blyth,[34] G.J.Bobbink,[2] A.Böhm,[1] L.Boldizsar,[12] B.Borgia,[38] S.Bottai,[17] D.Bourilkov,[46] M.Bourquin,[20] S.Braccini,[20] J.G.Branson,[40] F.Brochu,[4] J.D.Burger,[13] W.J.Burger,[32] X.D.Cai,[13] M.Capell,[13] G.Cara Romeo,[8] G.Carlino,[28] A.Cartacci,[17] J.Casaus,[24] F.Cavallari,[38] N.Cavallo,[35] C.Cecchi,[32] M.Cerrada,[24] M.Chamizo,[20] Y.H.Chang,[48] M.Chemarin,[23] A.Chen,[48] G.Chen,[7] G.M.Chen,[7] H.F.Chen,[21] H.S.Chen,[7] G.Chiefari,[28] L.Cifarelli,[39] F.Cindolo,[8] I.Clare,[13] R.Clare,[37] G.Coignet,[4] N.Colino,[24] S.Costantini,[38] B.de la Cruz,[24] S.Cucciarelli,[32] J.A.van Dalen,[30] R.de Asmundis,[28] P.Déglon,[20] J.Debreczeni,[12] A.Degré,[4] K.Dehmelt,[25] K.Deiters,[44] D.della Volpe,[28] E.Delmeire,[20] P.Denes,[36] F.DeNotaristefani,[38] A.De Salvo,[46] M.Diemoz,[38] M.Dierckxsens,[2] C.Dionisi,[38] M.Dittmar,[46] A.Doria,[28] M.T.Dova,[10,♯] D.Duchesneau,[4] M.Duda,[1] B.Echenard,[20] A.Eline,[18] A.El Hage,[1] H.El Mamouni,[23] A.Engler,[34] F.J.Eppling,[13] P.Extermann,[20] M.A.Falagan,[24] S.Falciano,[38] A.Favara,[31] J.Fay,[23] O.Fedin,[33] M.Felcini,[46] T.Ferguson,[34] H.Fesefeldt,[1] E.Fiandrini,[32] J.H.Field,[20] F.Filthaut,[30] P.H.Fisher,[13] W.Fisher,[36] I.Fisk,[40] G.Forconi,[13] K.Freudenreich,[46] C.Furetta,[26] Yu.Galaktionov,[27,13] S.N.Ganguli,[9] P.Garcia-Abia,[24] M.Gataullin,[31] S.Gentile,[38] S.Giagu,[38] Z.F.Gong,[21] G.Grenier,[23] O.Grimm,[46] M.W.Gruenewald,[16] M.Guida,[39] R.van Gulik,[2] V.K.Gupta,[36] A.Gurtu,[9] L.J.Gutay,[43] D.Haas,[5] D.Hatzifotiadou,[8] T.Hebbeker,[1] A.Hervé,[18] J.Hirschfelder,[34] H.Hofer,[46] M.Hohlmann,[25] G.Holzner,[46] S.R.Hou,[48] Y.Hu,[30] B.N.Jin,[7] L.W.Jones,[3] P.de Jong,[2] I.Josa-Mutuberría,[24] D.Käfer,[1] M.Kaur,[14] M.N.Kienzle-Focacci,[20] J.K.Kim,[42] J.Kirkby,[18] W.Kittel,[30] A.Klimentov,[13,27] A.C.König,[30] M.Kopal,[43] V.Koutsenko,[13,27] M.Kräber,[46] R.W.Kraemer,[34] A.Krüger,[45] A.Kunin,[13] P.Ladron de Guevara,[24] I.Laktineh,[23] G.Landi,[17] M.Lebeau,[18] A.Lebedev,[13] P.Lebrun,[23] P.Lecomte,[46] P.Lecoq,[18] P.Le Coultre,[46] J.M.Le Goff,[18] R.Leiste,[45] M.Levtchenko,[26] P.Levtchenko,[33] C.Li,[21] S.Likhoded,[45] C.H.Lin,[48] W.T.Lin,[48] F.L.Linde,[2] L.Lista,[28] Z.A.Liu,[7] W.Lohmann,[45] E.Longo,[38] Y.S.Lu,[7] C.Luci,[38] L.Luminari,[38] W.Lustermann,[46] W.G.Ma,[21] L.Malgeri,[20] A.Malinin,[27] C.Maña,[24] J.Mans,[36] J.P.Martin,[23] F.Marzano,[38] K.Mazumdar,[9] R.R.McNeil,[6] S.Mele,[18,28] L.Merola,[28] M.Meschini,[17] W.J.Metzger,[30] A.Mihul,[11] H.Milcent,[18] G.Mirabelli,[38] J.Mnich,[1] G.B.Mohanty,[9] G.S.Muanza,[23] A.J.M.Muijs,[2] B.Musicar,[40] M.Musy,[38] S.Nagy,[15] S.Natale,[20] M.Napolitano,[28] F.Nessi-Tedaldi,[46] H.Newman,[31] A.Nisati,[38] T.Novak,[30] H.Nowak,[45] R.Ofierzynski,[46] G.Organtini,[38] I.Pal,[43]C.Palomares,[24] P.Paolucci,[28] R.Paramatti,[38] G.Passaleva,[17] S.Patricelli,[28] T.Paul,[10] M.Pauluzzi,[32] C.Paus,[13] F.Pauss,[46] M.Pedace,[38] S.Pensotti,[26] D.Perret-Gallix,[4] B.Petersen,[30] D.Piccolo,[28] F.Pierella,[8] M.Pioppi,[32] P.A.Piroué,[36] E.Pistolesi,[26] V.Plyaskin,[27] M.Pohl,[20] V.Pojidaev,[17] J.Pothier,[18] D.Prokofiev,[33] J.Quartieri,[39] G.Rahal-Callot,[46] M.A.Rahaman,[9] P.Raics,[15] N.Raja,[9] R.Ramelli,[46] P.G.Rancoita,[26] R.Ranieri,[17] A.Raspereza,[45] P.Razis,[29]D.Ren,[46] M.Rescigno,[38] S.Reucroft,[10] S.Riemann,[45] K.Riles,[3] B.P.Roe,[3] L.Romero,[24] A.Rosca,[45] C.Rosenbleck,[1] S.Rosier-Lees,[4] S.Roth,[1] J.A.Rubio,[18] G.Ruggiero,[17] H.Rykaczewski,[46] A.Sakharov,[46] S.Saremi,[6] S.Sarkar,[38] J.Salicio,[18] E.Sanchez,[24] C.Schäfer,[18] V.Schegelsky,[33] H.Schopper,[47] D.J.Schotanus,[30] C.Sciacca,[28] L.Servoli,[32] S.Shevchenko,[31] N.Shivarov,[41] V.Shoutko,[13] E.Shumilov,[27] A.Shvorob,[31] D.Son,[42] C.Souga,[23] P.Spillantini,[17] M.Steuer,[13] D.P.Stickland,[36] B.Stoyanov,[41] A.Straessner,[20] K.Sudhakar,[9] G.Sultanov,[41] L.Z.Sun,[21] S.Sushkov,[1] H.Suter,[46] J.D.Swain,[10] Z.Szillasi,[25,¶] X.W.Tang,[7] P.Tarjan,[15] L.Tauscher,[5] L.Taylor,[10] B.Tellili,[23] D.Teyssier,[23] C.Timmermans,[30] Samuel C.C.Ting,[13] S.M.Ting,[13] S.C.Tonwar,[9] J.Tóth,[12] C.Tully,[36] K.L.Tung,[7]J.Ulbricht,[46] E.Valente,[38] R.T.Van de Walle,[30] R.Vasquez,[43] V.Veszpremi,[25] G.Vesztergombi,[12] I.Vetlitsky,[27] D.Vicinanza,[39] G.Viertel,[46] S.Villa,[37] M.Vivargent,[4] S.Vlachos,[5] I.Vodopianov,[25] H.Vogel,[34] H.Vogt,[45] I.Vorobiev,[34,27] A.A.Vorobyov,[33] M.Wadhwa,[5] Q.Wang[30] X.L.Wang,[21] Z.M.Wang,[21] M.Weber,[1] P.Wienemann,[1] H.Wilkens,[30] S.Wynhoff,[36] L.Xia,[31] Z.Z.Xu,[21] J.Yamamoto,[3] B.Z.Yang,[21] C.G.Yang,[7] H.J.Yang,[3] M.Yang,[7] S.C.Yeh,[49] An.Zalite,[33] Yu.Zalite,[33] Z.P.Zhang,[21] J.Zhao,[21] G.Y.Zhu,[7] R.Y.Zhu,[31] H.L.Zhuang,[7] A.Zichichi,[8,18,19] B.Zimmermann,[46] M.Zöller.[1]

1 III. Physikalisches Institut, RWTH, D-52056 Aachen, Germany[§]
2 National Institute for High Energy Physics, NIKHEF, and University of Amsterdam, NL-1009 DB Amsterdam, The Netherlands
3 University of Michigan, Ann Arbor, MI 48109, USA
4 Laboratoire d'Annecy-le-Vieux de Physique des Particules, LAPP,IN2P3-CNRS, BP 110, F-74941 Annecy-le-Vieux CEDEX, France
5 Institute of Physics, University of Basel, CH-4056 Basel, Switzerland
6 Louisiana State University, Baton Rouge, LA 70803, USA
7 Institute of High Energy Physics, IHEP, 100039 Beijing, China[△]
8 University of Bologna and INFN-Sezione di Bologna, I-40126 Bologna, Italy
9 Tata Institute of Fundamental Research, Mumbai (Bombay) 400 005, India
10 Northeastern University, Boston, MA 02115, USA
11 Institute of Atomic Physics and University of Bucharest, R-76900 Bucharest, Romania
12 Central Research Institute for Physics of the Hungarian Academy of Sciences, H-1525 Budapest 114, Hungary[‡]
13 Massachusetts Institute of Technology, Cambridge, MA 02139, USA
14 Panjab University, Chandigarh 160 014, India.
15 KLTE-ATOMKI, H-4010 Debrecen, Hungary[¶]
16 Department of Experimental Physics, University College Dublin, Belfield, Dublin 4, Ireland
17 INFN Sezione di Firenze and University of Florence, I-50125 Florence, Italy
18 European Laboratory for Particle Physics, CERN, CH-1211 Geneva 23, Switzerland
19 World Laboratory, FBLJA Project, CH-1211 Geneva 23, Switzerland
20 University of Geneva, CH-1211 Geneva 4, Switzerland
21 Chinese University of Science and Technology, USTC, Hefei, Anhui 230 029, China[△]
22 University of Lausanne, CH-1015 Lausanne, Switzerland
23 Institut de Physique Nucléaire de Lyon, IN2P3-CNRS,Université Claude Bernard, F-69622 Villeurbanne, France
24 Centro de Investigaciones Energéticas, Medioambientales y Tecnológicas, CIEMAT, E-28040 Madrid, Spain♭
25 Florida Institute of Technology, Melbourne, FL 32901, USA
26 INFN-Sezione di Milano, I-20133 Milan, Italy
27 Institute of Theoretical and Experimental Physics, ITEP, Moscow, Russia
28 INFN-Sezione di Napoli and University of Naples, I-80125 Naples, Italy
29 Department of Physics, University of Cyprus, Nicosia, Cyprus
30 University of Nijmegen and NIKHEF, NL-6525 ED Nijmegen, The Netherlands
31 California Institute of Technology, Pasadena, CA 91125, USA
32 INFN-Sezione di Perugia and Università Degli Studi di Perugia, I-06100 Perugia, Italy
33 Nuclear Physics Institute, St. Petersburg, Russia
34 Carnegie Mellon University, Pittsburgh, PA 15213, USA
35 INFN-Sezione di Napoli and University of Potenza, I-85100 Potenza, Italy
36 Princeton University, Princeton, NJ 08544, USA
37 University of Californa, Riverside, CA 92521, USA
38 INFN-Sezione di Roma and University of Rome, "La Sapienza", I-00185 Rome, Italy
39 University and INFN, Salerno, I-84100 Salerno, Italy
40 University of California, San Diego, CA 92093, USA
41 Bulgarian Academy of Sciences, Central Lab. of Mechatronics and Instrumentation, BU-1113 Sofia, Bulgaria
42 The Center for High Energy Physics, Kyungpook National University, 702-701 Taegu, Republic of Korea
43 Purdue University, West Lafayette, IN 47907, USA
44 Paul Scherrer Institut, PSI, CH-5232 Villigen, Switzerland
45 DESY, D-15738 Zeuthen, Germany
46 Eidgenössische Technische Hochschule, ETH Zürich, CH-8093 Zürich, Switzerland
47 University of Hamburg, D-22761 Hamburg, Germany
48 National Central University, Chung-Li, Taiwan, China
49 Department of Physics, National Tsing Hua University, Taiwan, China

§ Supported by the German Bundesministerium für Bildung, Wissenschaft, Forschung und Technologie
‡ Supported by the Hungarian OTKA fund under contract numbers T019181, F023259 and T037350.
¶ Also supported by the Hungarian OTKA fund under contract number T026178.
♭ Supported also by the Comisión Interministerial de Ciencia y Tecnología.
♯ Also supported by CONICET and Universidad Nacional de La Plata, CC 67, 1900 La Plata, Argentina.
△ Supported by the National Natural Science Foundation of China.

$\sqrt{s}$ (GeV)	Named as	$\mathcal{L}$ (pb^{-1})
188.6	189	176.0
191.6	192	29.5
195.5	196	83.9
199.5	200	81.3
201.7	202	34.8
202.5−205.5	205	74.8
205.5−207.2	207	130.2
207.2−209.2	208	8.6

Table 1: Centre-of-mass energies, naming convention and corresponding integrated luminosities.

	Single-Photon $P_t^{\gamma} > 0.02\sqrt{s}$		Single-Photon $P_t^{\gamma} < 0.02\sqrt{s}$ $P_t^{\gamma} > 0.008\sqrt{s}$		Multi-Photon $P_t^{\gamma\gamma} > 0.02\sqrt{s}$ $E_{\gamma} > 1$ GeV	
$\sqrt{s}$ (GeV)	Data	Expected	Data	Expected	Data	Expected
189	607	615.6	160	162.2	26	36.2
192	89	94.6	34	29.9	11	5.8
196	256	258.4	79	84.7	17	15.6
200	241	238.3	77	80.3	15	15.0
202	114	102.0	35	36.4	3	6.2
205	213	210.1	74	64.7	10	12.6
207	354	362.5	98	112.2	17	22.0
208	24	23.5	9	7.4	2	1.5
Total	1898	1905.1	566	577.8	101	114.8

Table 2: Numbers of observed and expected events selected in different kinematic regions for different values of $\sqrt{s}$.

	M_{rec} [GeV]					
$\lvert\cos\theta_{\gamma}\rvert$	0 − 70	70 − 95	95 − 120	120 − 145	145 − 170	170 − 210
0.000 − 0.200	1/0.5/82	55/52.9/88	34/38.5/87	18/16.8/88	26/23.6/82	66/74.8/73
0.200 − 0.400	1/0.5/80	48/65.5/89	49/40.1/89	31/16.8/85	22/25.6/84	93/79.2/73
0.400 − 0.600	0/0.4/81	67/81.8/88	57/54.9/88	24/22.2/87	33/32.2/83	91/90.0/73
0.600 − 0.730	0/0.6/79	82/68.2/84	44/54.2/84	27/19.9/83	26/29.2/81	76/68.7/68
0.800 − 0.870	0/0.7/80	82/83.0/93	59/60.2/93	28/26.2/91	24/31.2/85	66/58.7/47
0.870 − 0.920	0/0.7/76	100/91.9/91	61/65.9/90	26/25.5/86	30/32.8/78	51/50.4/37
0.920 − 0.953	0/0.5/60	94/97.3/87	61/69.9/84	28/24.7/79	20/24.9/57	31/32.8/22
0.953 − 0.972	0/0.3/59	82/78.9/70	47/52.7/68	24/20.4/64	12/16.5/36	1/ 2.2/ 3

Table 3: Numbers of events selected by the high energy single-photon selection, Standard Model expectations and selection efficiencies in % as a function of the recoil mass, M_{rec}, and of the photon polar angle, $\lvert\cos\theta_{\gamma}\rvert$. The phase space region corresponding to this selection is defined in the text.

	M_{rec} [GeV]					
$E_{\gamma 2}$ [GeV]	$0-70$	$70-95$	$95-120$	$120-150$	$150-180$	$180-210$
Full sample						
$0-15$	0/0.2/59	34/30.6/60	19/21.1/61	9/10.3/58	13/17.6/54	7/7.4/39
$15-40$	0/0.1/64	12/12.4/52	5/ 8.2/55	2/ 3.2/54	0/ 0.9/59	—
$40-80$	0/0.2/62	0/ 1.9/60	0/ 0.5/54	—	—	—
Both Photons in $43^\circ < \theta_\gamma < 137^\circ$						
$0-15$	0/0.1/74	5/6.0/71	4/4.7/78	2/2.1/69	2/4.5/65	1/2.1/45
$15-40$	0/0.0/75	6/3.2/69	1/2.1/77	0/1.0/80	0/0.3/75	—
$40-80$	0/0.2/68	0/0.7/73	0/0.1/75	—	—	—

Table 4: Numbers of observed and expected multi-photon events and selection efficiencies in % as a function of M_{rec} and $E_{\gamma 2}$ for the full sample and for the case in which both photons are in the barrel. The phase space region corresponding to the multi-photon selection is defined in the text.

	x_γ													
$\lvert\cos\theta_\gamma\rvert$	$0.00-0.02$		$0.02-0.03$		$0.03-0.05$		$0.05-0.10$		$0.10-0.20$		$0.20-0.35$		$0.35-0.50$	
$0.00-0.20$	29	19.8	39	39.5	25	20.7	28	28.5	22	29.7	24	22.5	13	14.5
	28	17	54	31	64	86	68	99	79	99	82	99	83	99
$0.20-0.40$	31	30.3	57	52.8	27	23.8	36	29.4	36	32.0	20	25.8	17	15.1
	33	11	53	24	63	83	68	99	79	99	83	99	84	99
$0.40-0.60$	19	17.3	111	105.9	55	57.4	36	36.8	44	37.6	28	30.4	21	19.7
	36	11	50	13	63	41	67	97	78	98	83	99	84	99
$0.60-0.73$	—		111	135.8	83	90.7	27	28.1	34	32.3	34	27.0	17	18.0
	—		51	8	59	22	57	94	73	99	79	99	81	99
$0.87-0.92$	—		—		—		12	17.8	82	67.6	42	57.3	50	41.9
	—		—		—		17	96	73	99	78	99	84	98
$0.92-0.97$	—		—		—		—		18	23.4	24	29.8	31	32.9
	—		—		—		—		21	94	38	100	58	100

Table 5: Numbers of observed and expected single-photon events, together with selection efficiencies and purities in % as a function of the ratio of the photon energy to the beam energy, x_γ, and $\lvert\cos\theta_\gamma\rvert$. Results from the combined high and low energy selections are shown. The phase space regions corresponding to these selections are defined in the text. In the first row of each cell, the left number represents the number of observed events and the right number the expectations from Standard Model processes. In the second row of each cell, the left number is the selection efficiency and the right number the purity.

$\sqrt{s}$ (GeV)	ε(%)	$\sigma_{measured}$ (pb)	$\sigma_{expected}$ (pb)
189	73.7 ± 0.2	$4.83 \pm 0.19 \pm 0.05$	4.97
192	71.0 ± 0.2	$4.75 \pm 0.48 \pm 0.05$	4.77
196	70.9 ± 0.2	$4.56 \pm 0.28 \pm 0.05$	4.58
200	70.4 ± 0.2	$4.44 \pm 0.28 \pm 0.05$	4.39
202	70.4 ± 0.2	$4.73 \pm 0.44 \pm 0.05$	4.37
205	70.3 ± 0.2	$4.20 \pm 0.28 \pm 0.05$	4.20
207	70.6 ± 0.2	$4.00 \pm 0.21 \pm 0.05$	4.15
208	69.8 ± 0.2	$4.29 \pm 0.85 \pm 0.05$	4.12

Table 6: Combined trigger and selection efficiency, ε, and measured, $\sigma_{measured}$, and expected, $\sigma_{expected}$, cross sections as a function of $\sqrt{s}$ for the $e^+e^- \rightarrow \nu\bar{\nu}\gamma(\gamma)$ process in the phase space region defined in the text. The statistical uncertainty on the selection efficiency is quoted. The first uncertainty on $\sigma_{measured}$ is statistical, the second systematic. The theoretical uncertainty on $\sigma_{expected}$ is 1% [?].

Source	Uncertainty (%)
Trigger efficiency	0.6
Monte Carlo modelling	0.6
Selection of converted photons	0.5
Photon identification	0.3
Monte Carlo statistics	0.3
Luminosity	0.2
Background level	0.2
Cosmic contamination	0.1
Calorimeter calibration	0.1
Total	1.1

Table 7: Systematic uncertainties on the measurement of the $e^+e^- \rightarrow \nu\bar{\nu}\gamma(\gamma)$ cross section.

n	$(1/M_D)^{n+2}$	M_{D95} (TeV)	M_{exp} (TeV)	R_{95} (cm)
2	-0.03 ± 0.10 TeV^{-4}	1.50	1.49	2.1×10^{-2}
3	-0.10 ± 0.28 TeV^{-5}	1.14	1.12	2.9×10^{-7}
4	-0.5 ± 1.0 TeV^{-6}	0.91	0.89	1.1×10^{-9}
5	-2.2 ± 3.9 TeV^{-7}	0.76	0.75	4.2×10^{-11}
6	-11.2 ± 17.7 TeV^{-8}	0.65	0.64	4.7×10^{-12}
7	-67 ± 87 TeV^{-9}	0.57	0.56	1.0×10^{-12}
8	-400 ± 460 TeV^{-10}	0.51	0.51	3.2×10^{-13}

Table 8: Fitted values of $(1/M_D)^{n+2}$, together with the observed, M_{D95}, and expected, M_{exp}, lower limits on the gravity scale as a function of the number of extra dimensions, n. Upper limits on the size of the extra dimensions, R_{95}, are also given. All limits are at the 95% confidence level.

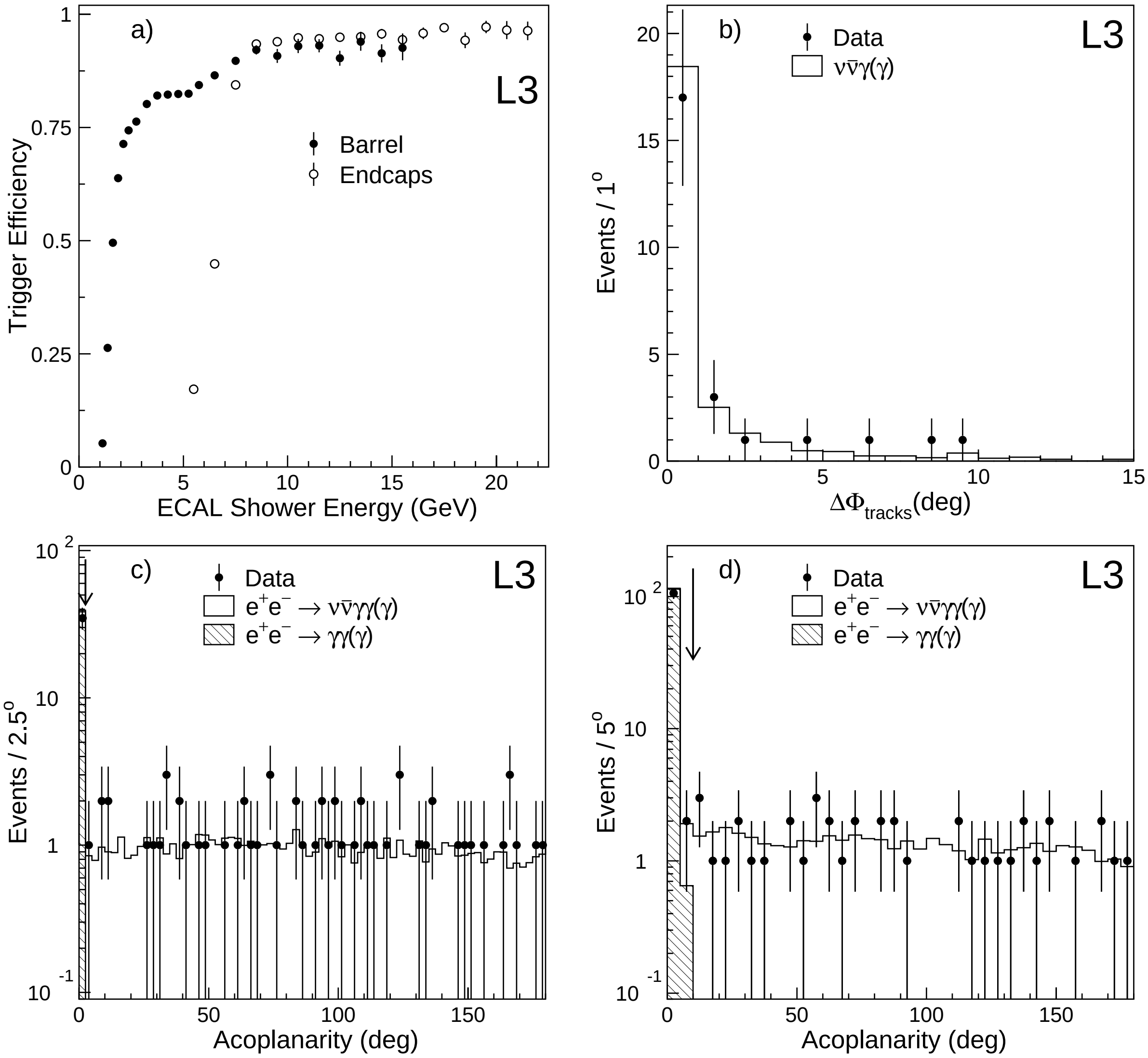

Figure 1: a) Trigger efficiency as a function of the ECAL shower energy. Distributions of: b) the azimuthal angle between two matching tracks for photons accepted by the conversion selection in the barrel, c) the acoplanarity between the two most energetic photons for ECAL showers which are not near the calorimeter edges and do not contain dead channels, and d) for the case when at least one of the showers does not satisfy these conditions. The arrows indicate the values of the cuts.

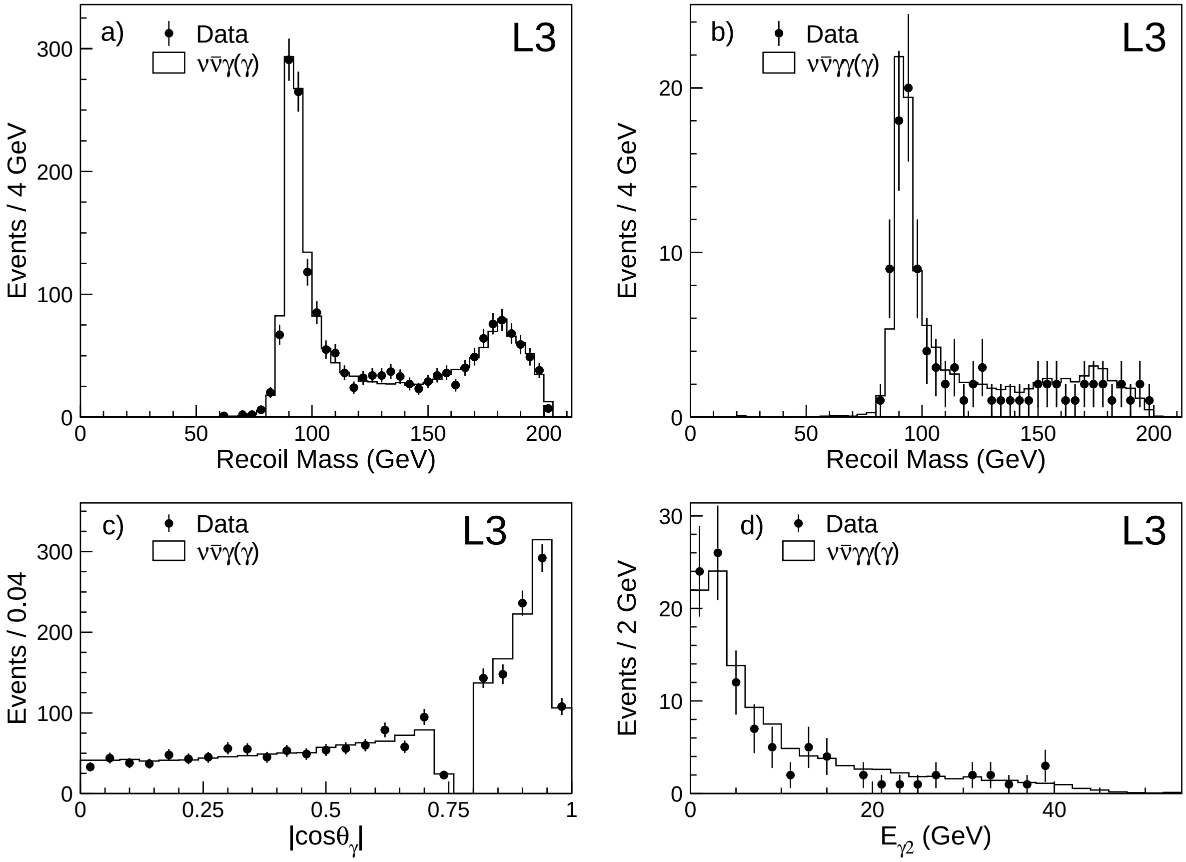

Figure 2: Distributions of a) the recoil mass and c) the polar angle for the high energy single-photon events and of b) the recoil mass and d) the energy of the second most energetic photon for the multi-photon sample.

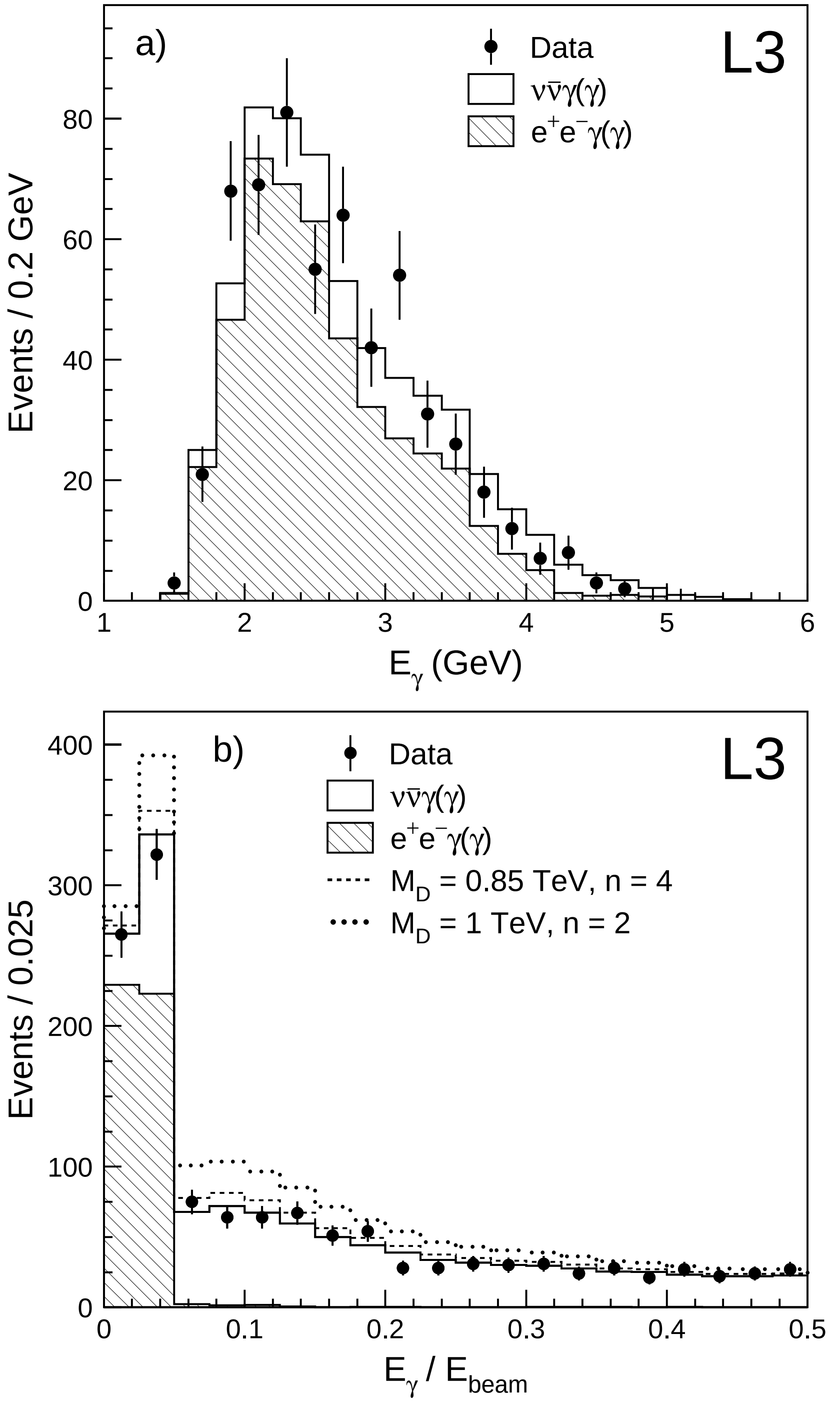

Figure 3: Distributions of a) the photon energy for the low energy single-photon selection and b) the ratio of the photon energy to the beam energy, x_γ, for single-photon events from the combined high and low energy single-photon selections. Signals for extra dimensions for $M_D = 1$ and 0.85 TeV and $n = 2$ and 4 are also shown.

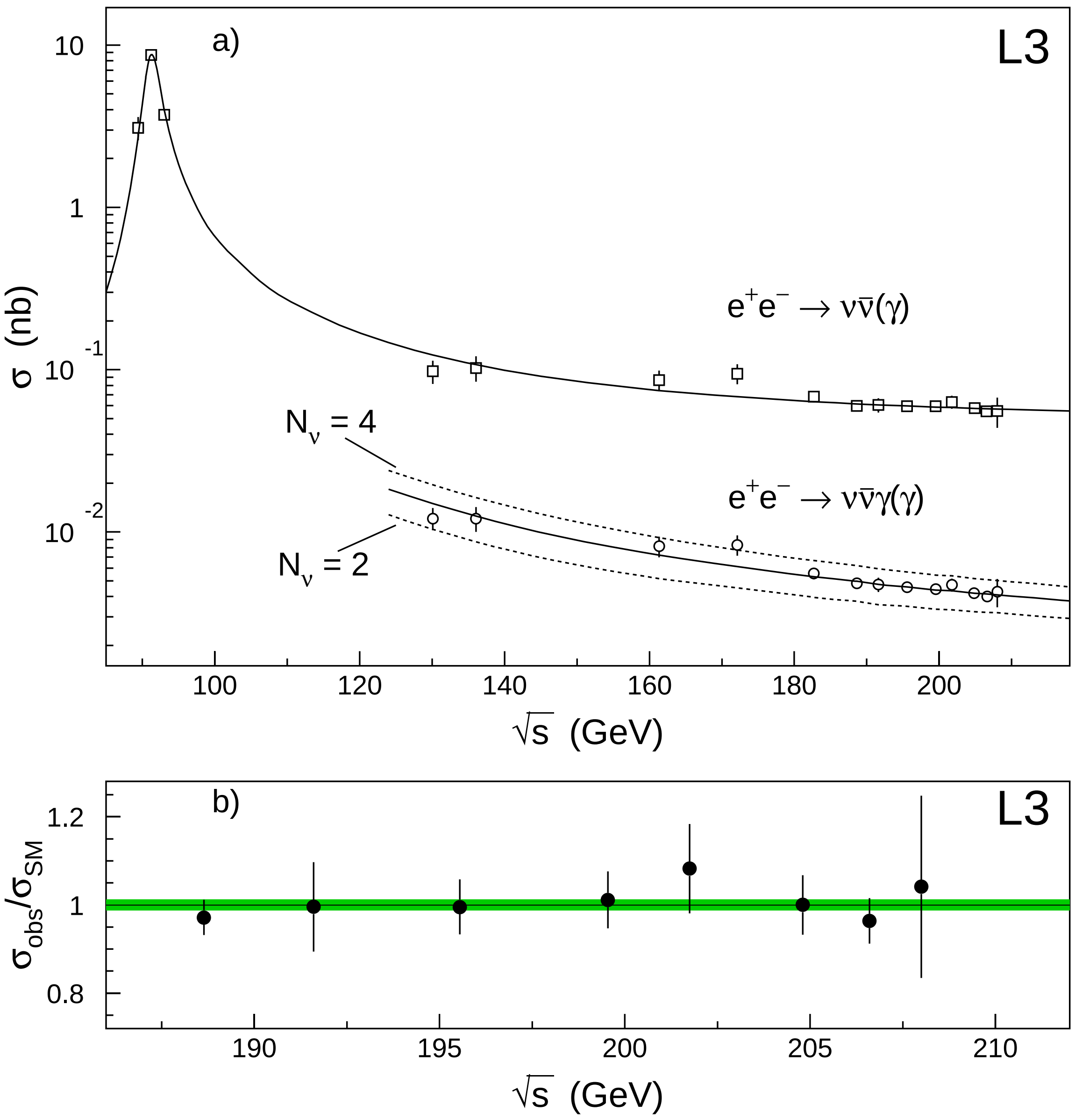

Figure 4: a) Cross sections of the $e^+e^- \to \nu\bar{\nu}(\gamma)$ and $e^+e^- \to \nu\bar{\nu}\gamma(\gamma)$ processes as a function of $\sqrt{s}$. The cross section of the latter process refers to the kinematic region defined in the text. The full line represents the theoretical prediction for $N_\nu = 3$ and the dashed lines are predictions for $N_\nu = 2$ and 4, as indicated. b) The ratio of the measured and the Standard Model predicted cross sections as a function of $\sqrt{s}$. The shaded region represents the theoretical uncertainty of 1% [?].

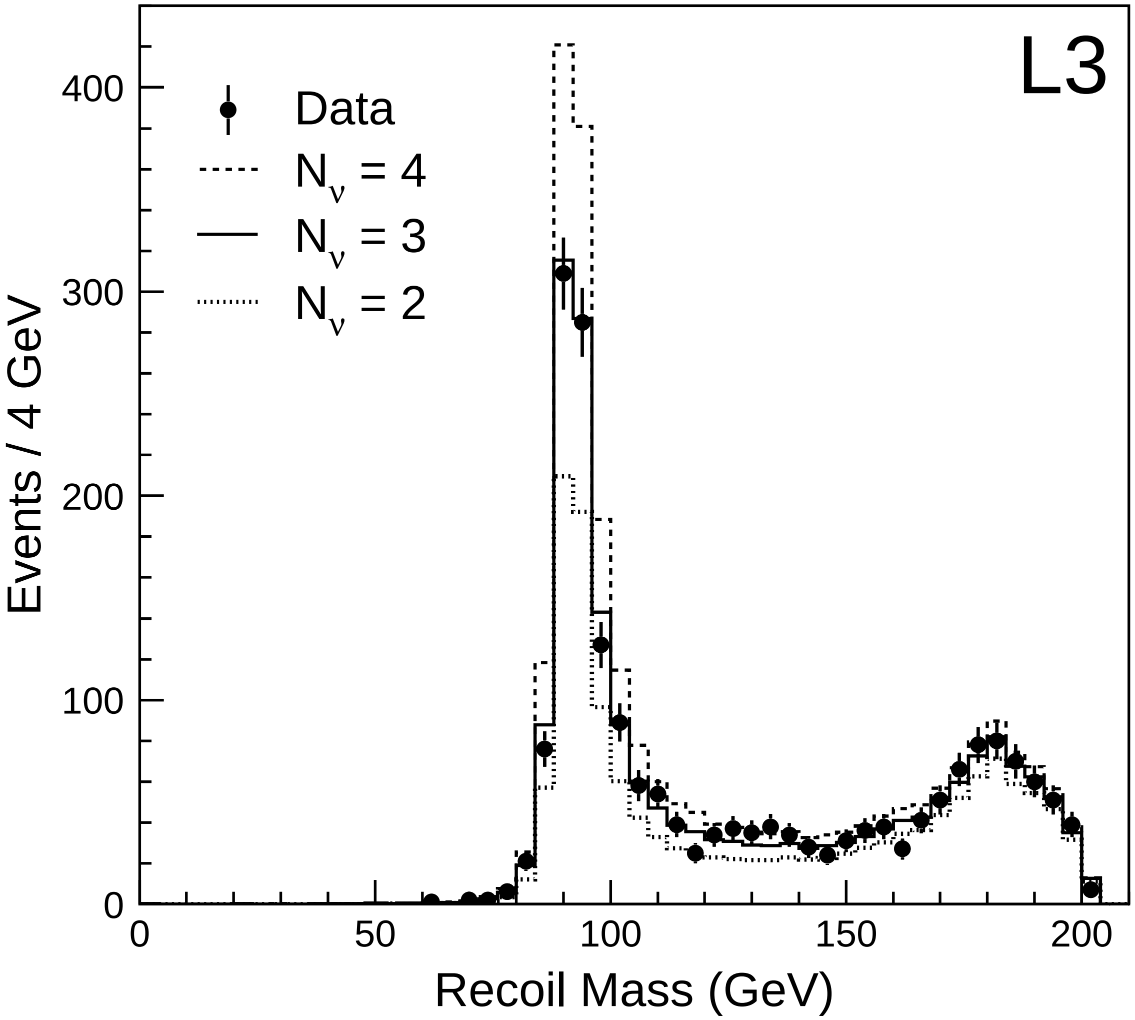

Figure 5: The recoil mass spectrum of the single- and multi-photon events compared to the expected spectra for $N_\nu = 2, 3$ and 4.

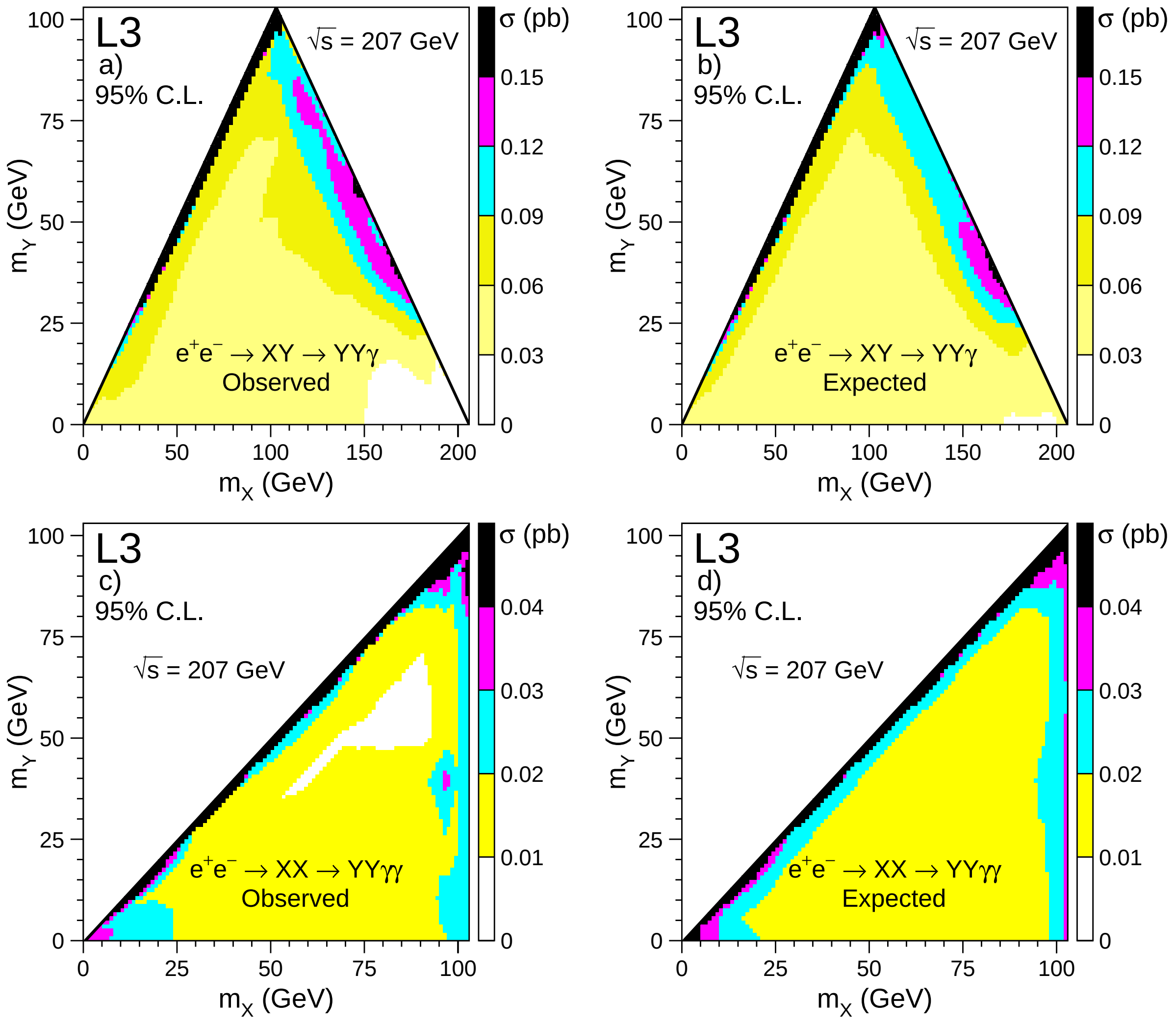

Figure 6: Cross section upper limits at 95% confidence level for model-independent searches: a) observed and b) expected for the process $e^+e^- \rightarrow XY \rightarrow YY\gamma$ and c) observed and d) expected for the process $e^+e^- \rightarrow XX \rightarrow YY\gamma\gamma$. The limits are obtained for $\sqrt{s} = 207$ GeV. Data collected at lower $\sqrt{s}$ are included assuming the signal cross sections to scale as β_0/s, where β_0 is defined in the text.

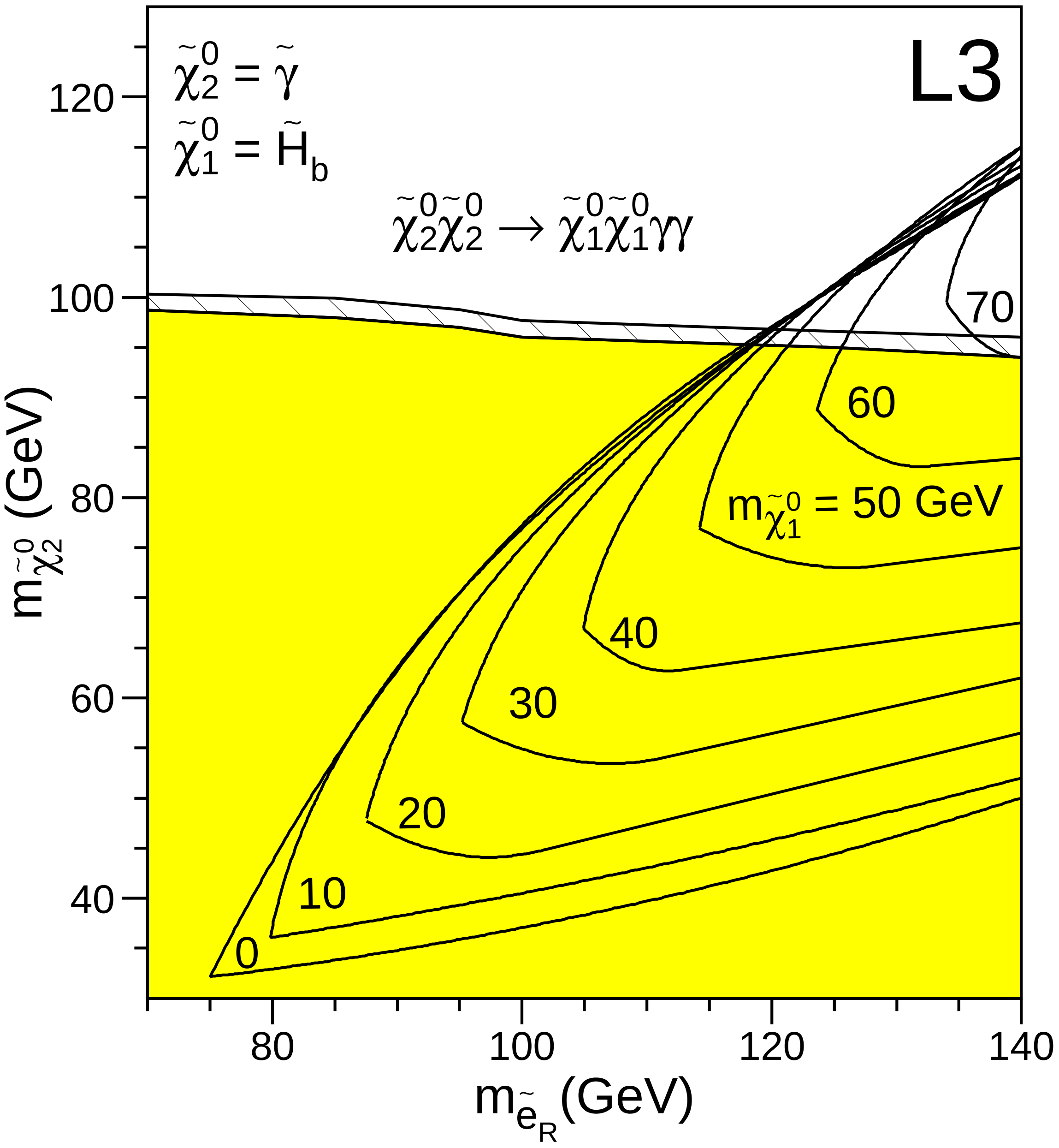

Figure 7: Region excluded at 95% confidence level in the $m_{\tilde{\chi}_2^0}$ *vs.* $m_{\tilde{e}_R}$ plane. The shaded region corresponds to $m_{\tilde{e}_L} \gg m_{\tilde{e}_R}$ and the hatched region is additionally excluded when $m_{\tilde{e}_L} = m_{\tilde{e}_R}$. The mass difference between $\tilde{\chi}_2^0$ and $\tilde{\chi}_1^0$ is assumed to be greater than 10 GeV. Regions kinematically allowed for the CDF event [**?**] as a function of $m_{\tilde{\chi}_1^0}$ are also indicated.

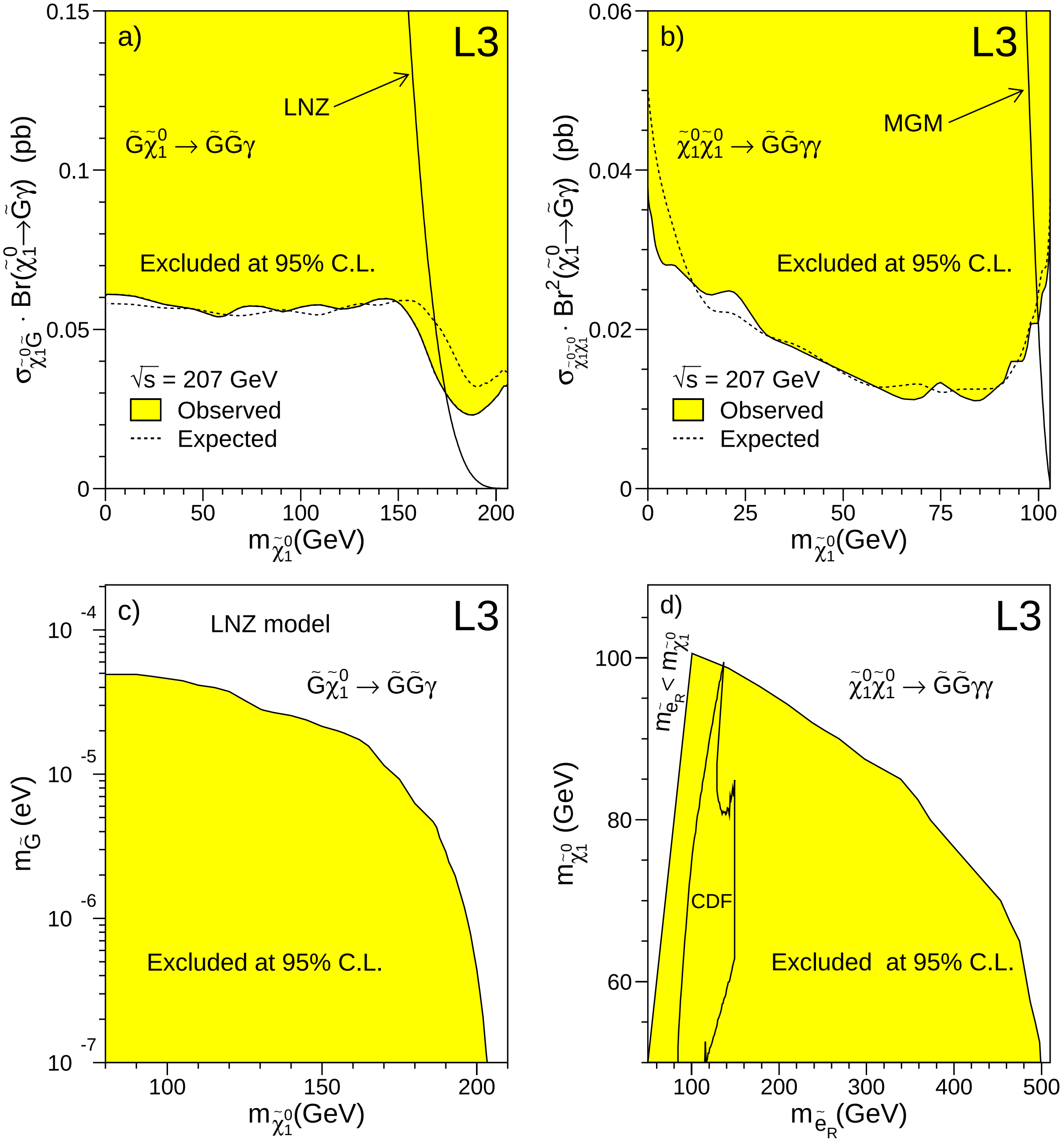

Figure 8: Observed and expected 95% confidence level upper limits at $\sqrt{s} = 207$ GeV on the production cross section for the processes a) $\mathrm{e^+e^-} \to \tilde{\mathrm{G}}\tilde{\chi}^0_1 \to \tilde{\mathrm{G}}\tilde{\mathrm{G}}\gamma$ and b) $\mathrm{e^+e^-} \to \tilde{\chi}^0_1\tilde{\chi}^0_1 \to \tilde{\mathrm{G}}\tilde{\mathrm{G}}\gamma\gamma$. The cross section predicted by the LNZ model [?] for $m_{\tilde{\mathrm{G}}} = 10^{-5}$ eV is also shown in a), while the prediction of the MGM model is shown in b). Regions excluded for c) the LNZ model in the $m_{\tilde{\mathrm{G}}}$ *vs.* $m_{\tilde{\chi}^0_1}$ plane, and for d) a pure bino neutralino model in the $m_{\tilde{\chi}^0_1}$ *vs.* $m_{\tilde{\mathrm{e}}_\mathrm{R}}$ plane. The interpretation of the CDF event in the scalar electron scenario [?] is also shown in d).